Digital Microfluidics and Radiochemistry: Current State and Future Trends

Jay M. Pimprikar, Fatemeh Ahmadi, and Steve C. C. Shih

1 Need for Microscale Synthesis for Radiochemistry

Due to the high equipment and infrastructure costs associated with radioisotope synthesis and radiation shielding, the production of radiotracers, such as 2-[^{18}F]fluoro-2-deoxy-D-glucose ([^{18}F]FDG), used in Positron Emission Tomography (PET) scans, is typically centralized. A centralized approach provides a significant financial advantage for this tracer, since the expenses for producing this tracer can be spread among many patients with minimal additional costs incurred when scaling up the production. However, the limitation of centralized facilities is exacerbated, when the half-life is too short for transport (e.g., [^{11}C]Met) and when there is a need to obtain a diverse library of probes. Since most non-[^{18}F]FDG radiotracers are relatively low in demand, these tracers could not be provided by a centralized radiopharmacy at a reasonable price that is affordable by any laboratory. Therefore, this has prompted the development of decentralized solutions, such as microfluidic "lab-on-chip" platforms, where imaging centers (located in local hospitals) can synthesize individual doses of various types of tracers in an automated and time-sensitive manner themselves (Chen et al., 2014a, 2014b; Vaquero & Kinahan, 2015).

Several microfluidic, decentralized, solutions have been developed to robustly synthesize PET tracers. Each of these solutions can be classified as a subset of the microfluidic paradigm they leverage: continuous-flow (Liang et al., 2014a, 2014b; Calderwood et al., 2015; Selivanova et al., 2012; Kimura et al., 2016),

J. M. Pimprikar · F. Ahmadi · S. C. C. Shih (✉)
Centre for Applied Synthetic Biology, Concordia University, Montréal, QC, Canada

Department of Electrical and Computer Engineering, Concordia University, Montréal, QC, Canada
e-mail: steve.shih@concordia.ca

R. M. van Dam et al. (eds.), *Automated Technologies for the Development and Production of Radiopharmaceuticals*,
https://doi.org/10.1007/978-3-031-84632-8_11

batch-reactor-based (Zhang et al., 2018; Bejot et al., 2011; Lebedev et al., 2013; Elizarov et al., 2010; Lee et al., 2005), and digital microfluidics (DMF) (Keng et al., 2012; Chen et al., 2014a, 2014b; Javed et al., 2014; Wang et al., 2019; Mogi et al., 2021; Ahmadi et al., 2023). Continuous-flow solutions struggle with cross-contamination (small amounts of previous fluids remain on the channel and are introduced into a new sample), leakage, clogging, and the need for conventional purification (Gillies et al., 2006; Audrain, 2007). While batch-reactor-based solutions have made progress in overcoming some of the drawbacks of continuous-flow solutions, certain challenges continue to persist. The high vapor pressure of solvents, resulting from the required increase in temperature, along with reagent evaporation, complex chip design and fabrication, and the complexity of external valve and pump control systems, act as barriers for the widespread adoption of this method at localized facilities (Gillies et al., 2006; Lebedev et al., 2013; Elizarov et al., 2010).

2 Digital Microfluidic Automation and Operations

Digital microfluidics (DMF) is an electrode array-based platform that allows the manipulation of individual droplets through the application of an electric potential, eliminating the need for pumps or valves (Choi et al., 2012; Li, 2020; Liu et al., 2023). The benefits of DMF include "plug-and-play" automation, where the device can be directly connected to automation equipment, enabling programmable fluidic operations such as dispense, merge, mix, and split (Fig. 1a) (Moazami et al., 2019; Fobel et al., 2013) and reducing concerns of cross-contamination via routing of droplet movements along different electrode paths (Huang et al., 2010). The most common format for a DMF system is a two-plate system, where the droplet is sandwiched between the actuation (bottom) plate and the hydrophobically coated ground top plate (Fig. 1b). The bottom plate consists of metal-based electrodes where potentials are applied, upon which a dielectric insulator is coated on top to allow for charge insulation and polarization. This is followed by a hydrophobic layer to permit droplet mobility and reducing the friction between the droplet and the surface of the device. The architecture of the open DMF system is similar to that of the closed except the ground electrode is coplanar with the activated electrodes (Fig. 1b).

The mechanisms of DMF via applying an electric field to enable droplet actuation allows for pL to μL droplet mixing, merging, dispensing from on-chip reservoirs (i.e., electrodes that hold more volume than the typical actuation electrode), and splitting in an automated fashion (see review papers Choi et al., 2012; Li, 2020). Aside from these standard droplet operations, the radiochemistry applications performed on DMF require other non-droplet operations. First, temperature control is critical for many chemical processes, especially for radiochemical synthesis (Keng & van Dam, 2015; Chen et al., 2012a, 2012b, 2014a, 2014b; Ding et al., 2012; Javed et al., 2014; Keng et al., 2012; Mogi et al., 2021; Ahmadi et al., 2023), as the reactions need heat to accelerate the reaction kinetics and to limit the time for reactions involving isotopes with short half-lives. Generally, microheaters or thermoelectric

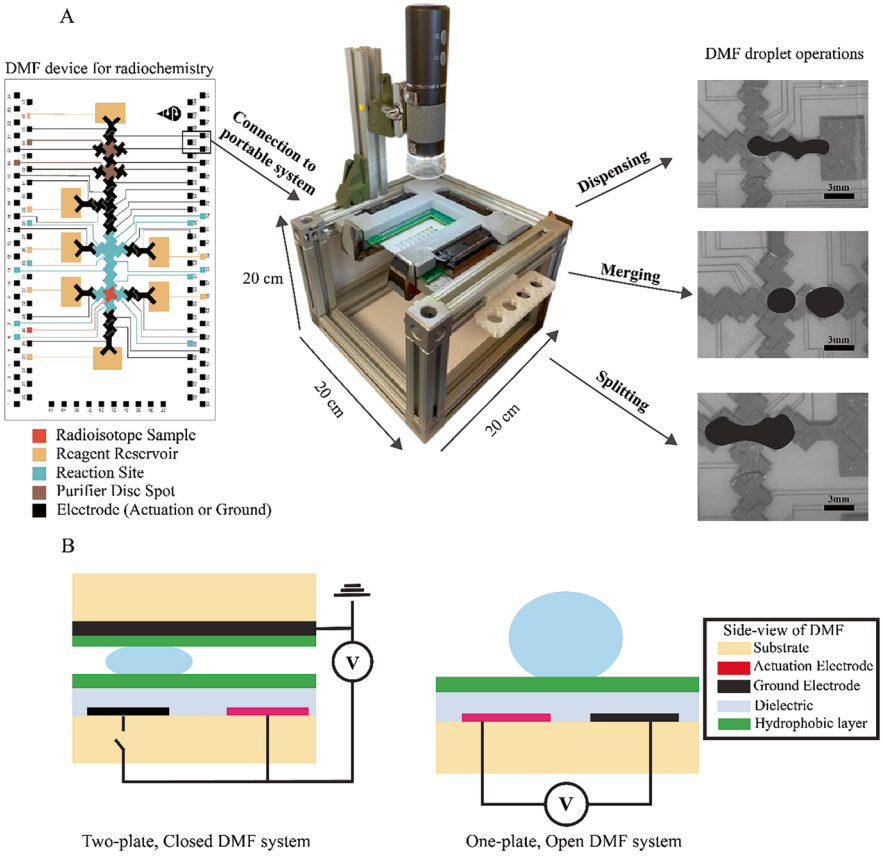

Fig. 1 Digital microfluidics for radiochemistry. (**a**) An automated digital microfluidic system for radiochemistry. To automate radiochemistry using DMF, a DMF device (left) requires a section for the radioisotope sample (red), the reaction site (cyan), and purification of the product (brown). Reagent reservoirs (gold) are used to dispense droplets of nL–μL volumes, which are then moved to different sections of the device by applying electric potentials to the electrodes (black). Application of the potentials are applied to devices via contact pads (rectangle) and are placed in a portable system (Perry et al., 2021) that can be used for decentralized synthesis. Using such a system, we can perform a number of droplet operations: mix, merge, and dispense as shown by the images from a movie (right) taken from Ahmadi et al., 2023 with permission from the Royal Society of Chemistry. (**b**) Side-view illustrations of two different DMF configurations. The two-plate, closed system includes a top, ground plate which is used to complete the actuation circuit. The one-plate system is open to atmosphere, and both ground and active electrodes are on the same plane

elements can be integrated on the bottom substrate along with a temperature sensor to continually monitor the temperature on the device. Reading the sensor temperature allows the execution of an algorithm, enabling precise temperature control through a closed-loop control system (Fig. 2a) (Moazami et al., 2019). Second, heating may cause sample evaporation and volume losses, and therefore a solution

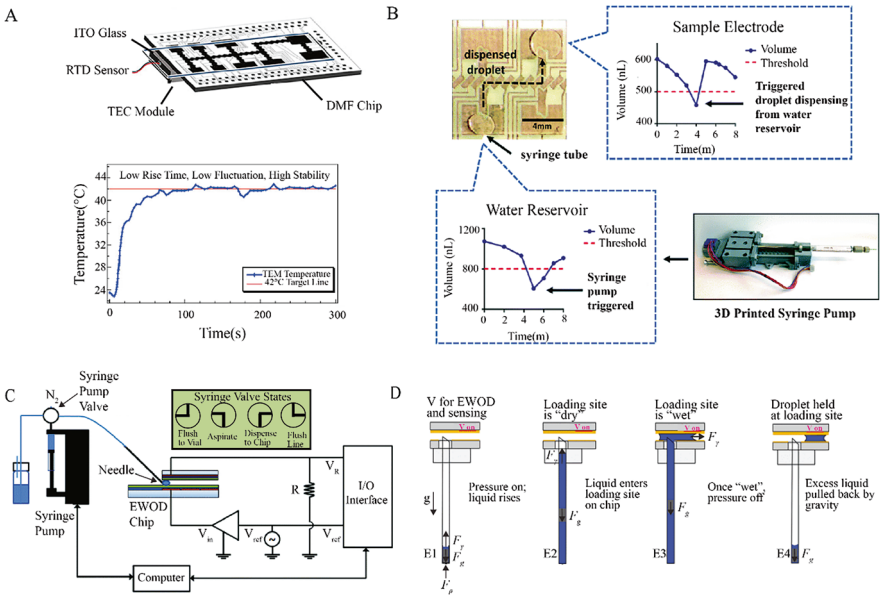

Fig. 2 DMF automation. (**a**) Temperature sensing on a DMF platform via integration of a thermoelectric cooler (TEC) module and a resistance temperature detector (RTD) sensor. Permission obtained from American Chemical Society. (**b**) 3D printed syringe pump-based replenishment system to mitigate evaporation on a DMF device (Perry et al., 2021). Permission obtained from the Royal Society of Chemistry. (**c**) Integration of on-chip impedance sensing for reagent delivery on a DMF chip (Ding et al., 2012) with permission from the Royal Society of Chemistry. (**d**) Stepwise workflow of pressure-based "world-to-chip" reagent delivery juxtaposing counteracting gravity (Shah et al., 2013). (Permission obtained from the Royal Society of Chemistry)

is to continually replenish and resupply samples with water to maintain the initial reaction concentrations. Several methods have been developed (Jebrail et al., 2015; Perry et al., 2021; Shah et al., 2013), but the most common method is to connect a syringe pump with the replenishment solution directly to an on-chip reservoir, which will then follow with typical droplet operations to replenish the sample volume (Fig. 2b). Third, evaporating solvent is a required operation for radiochemical synthesis which can be performed on the DMF device. The droplets are directly exposed to ambient air enables droplets being delivered to target areas where the droplets can evaporate directly on the device surface (Moon et al., 2006; Jebrail et al., 2010).

With its advanced automation capabilities, there exists significant potential in using DMF as a decentralized platform for radiotracer synthesis. This chapter is dedicated to a comprehensive exploration of the recent achievements and obstacles encountered in the integration of DMF into radiotracer synthesis processes. It particularly emphasizes the diverse array of operations achievable on DMF, encompassing both droplet and non-droplet techniques. Furthermore, we delve into the

exciting prospects that lie ahead by synergizing DMF with the evolution of radiotracer development.

3 Current Works in DMF and Radiochemistry

Prior to performing synthesis on-chip, specific radiochemical reagent dispensing techniques have been implemented to move toward full automation capabilities. Ding et al. used a syringe pump system to automate the delivery of acetonitrile (MeCN) during [^{18}F]FDG synthesis. Since MeCN is a "wetting" liquid (contact angle less than 90°), storing it on a chip reservoir is not possible (Ding et al., 2012; Shah et al., 2013) due to its rapid evaporation rate. To account for evaporation that may take place between dispensing the MeCN and it reaching the chip via a needle, an on-chip liquid detector was generated based on impedance sensing between the loading electrode and the ground electrode. The sensing took place via the integration of a 1 kΩ resistor between the ground plate and the power supply ground, whereupon the activation of the loading electrode generates an alternating current and voltage drop across the resistor (Ding et al., 2012). Figure 2c shows the integration of the 1 kΩ resistor serving as an impedance sensor and how it can be implemented for delivering accurate volumes of volatile liquids commonly used in radiotracer synthesis.

Alternatively, to having a bulky syringe pump for loading each liquid, Shah et al. used a combination of compressed inert gas and gravity to exert driving and retracting forces for precise loading of wetting and non-wetting liquids on-chip via a feedback signal (Shah et al., 2013). Wetting liquids such as MeCN necessitate a "world-to-chip" solution for dispensing, and the authors curated a pneumatic liquid loading system against gravity. The liquids are drawn from pierced septum-capped vials and delivered from underneath the actuation plate, so that gravity serves as a counteracting force to the pressurized vial (Shah et al., 2013). Figure 2d provides a workflow schematic of pneumatic liquid delivery "world-to-chip" system.

The most widely automated PET radiotracer on DMF has been [^{18}F]FDG due to its broad use in cancer imaging (Ashraf & Goyal, 2023). The chemical reaction fluorinates the precursor (mannose triflate) to generate intermediate [^{18}F]FTAG, and, upon hydrolysis, [^{18}F]FDG is produced (Fig. 3a). However, many other ^{18}F-based tracers, such as [^{18}F]FLT, [^{18}F]fallypride, [^{18}F]SFB, and the Single Photon Emission Computed Tomography (SPECT) tracer [^{99m}Tc]Tc-DTPA have also been synthesized using a similar DMF platform (Keng & van Dam, 2015; Mogi et al., 2021). For example, Fig. 3b shows the synthesis steps for [^{18}F]fallypride, which also requires the necessary steps (liquid handling, heating, drying) for successful production. As illustrated in Fig. 3c, [^{18}F]fallypride and other tracers ([^{18}F]FDG, [^{18}F]SFB, [^{18}F]FLT) can be synthesized using a single DMF chip design, as demonstrated by Chen et al. (2014a, 2014b). In this design, patterned square electrodes are fabricated for automating the liquid handling steps, and a concentric electrode design is used for heating, while Ahmadi et al. (2023) use the patterned electrodes

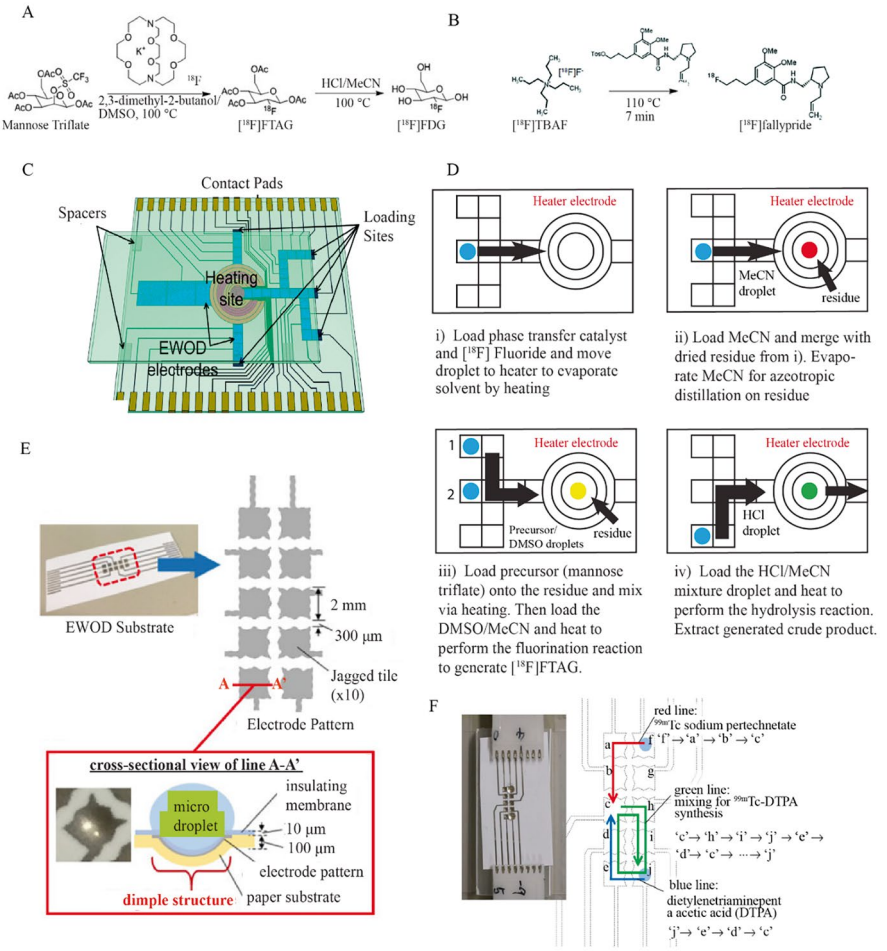

Fig. 3 Current DMF platforms for radiochemistry. (**a**) Schematic for multistep FDG synthesis via mannose triflate fluorination (Koag et al., 2014a, 2014b). Permission obtained from Elsevier. (**b**) Synthesis schematic of [^{18}F]fallypride (Wang et al., 2020). Permission obtained from the Royal Society of Chemistry. (**c**) Schematic of EWOD chip used for the synthesis of [^{18}F]FDG, [^{18}F]FLT, [^{18}F]fallypride, and [^{18}F]SFB (Chen et al., 2014a, 2014b). Permission obtained from the Royal Society of Chemistry. (**d**) Sample DMF FDG synthesis schematic adapted from Chen et al. (2014a, 2014b) and Keng and van Dam (2015) with permission from the Royal Society of Chemistry and the Proceedings of the National Academy of Sciences. (**e**) Schematic of a paper-based EWOD device showing electrode pattern and a cross-sectional view of the dimple structure (Mogi et al., 2021). Permission obtained from the Royal Society of Chemistry. (**f**) Schematic for the synthesis of [^{99m}Tc]Tc-DTPA on paper-based coplanar EWOD device (Mogi et al., 2021). (Permission obtained from the Royal Society of Chemistry)

exclusively for liquid handling and incorporate the heater externally to the substrate. In either case, droplets containing the precursors are dispensed, merged, mixed using the electrodes, and these droplets are further dried heated to expedite the

fluorination labeling process at a target electrode location, and then extracted off the chip (Fig. 3d).

The above devices are generally fabricated by patterning metal on a glass substrate coated with a dielectric and a hydrophobic layer (Keng et al., 2012; Chen et al. 2014b; Ahmadi et al., 2023). Glass (and silicon) substrate devices pose a challenge, as they require fabrication in cleanroom environments, hindering scalability and rendering them economically impractical for low-cost decentralized synthesis. However, an alternative substrate that could address this issue is paper. Recently, paper microfluidics and DMF have been combined (Abadian et al., 2017; Ruecha et al., 2017), leveraging the automation capabilities of DMF along with the numerous advantages offered by paper microfluidics. An example of this is the work by Mogi et al., who created an alternative open-style DMF device comprising a primarily paper substrate incorporated with dimple-based electrode structures to minimize any erroneous movements during the synthesis of SPECT tracer [^{99m}Tc]Tc-DTPA (Mogi et al., 2021). Droplets were manipulated by voltage switching using a palm-sized controller and the device consisted of 2 mm × 2 mm electrode patterns inkjet printed with conductive ink (Mogi et al., 2021). Figure 3e demonstrates the electrode patterns and cross-sectional layout of the device. As shown, a 10-μm-thick insulating membrane was layered and embossed on top of the electrodes to create the dimple patterns (Mogi et al., 2021). The adhesion energy was determined to be equal to 1.3 times that of a flat surface, creating dimples with depth of 52.9 ± 2.5 μm. This adhesion energy provided the best balance between droplet mobility and stability in dimple structures. Droplet manipulation was subsequently possible for volumes between 5 and 30 μL (Mogi et al., 2021). Using such a device, the SPECT tracer [^{99m}Tc]Tc-DTPA was synthesized on chip by mixing 10 μL of DTPA saline solution with 10 μL of sodium pertechnetate and incubating the mixture for 5 min at room temperature, as shown in Fig. 3f. After incubation, the chelating efficiency of [^{99m}Tc]Tc-DTPA was evaluated using TLC and determined to be 99.7 ± 0.13% (Mogi et al., 2021).

3.1 Improving Fluorination Efficiency and Radiochemical Yield

The primary goal of miniaturizing radiosynthesis, which encompasses reducing synthesis costs, time, and enabling decentralization, also hinges on achieving both a high crude radiochemical yield (RCY) and a high fluorination efficiency percentage. A high fluorination efficiency indicates a significant proportion of [^{18}F]fluoride has been successfully labeled on the precursor molecule, which is assessed by performing radio-HPLC analysis (Walters et al., 2012). Generally, if the fluorination step is highly efficient, it will lead to a higher amount of the radiotracer product in the final synthesis, positively impacting the crude RCY. However, several parameters such as reagent concentration, droplet volume, phase transfer catalyst

(PTC)-to-precursor ratio, fluorination reaction temperature, and reaction time require optimization such that maximum fluorination efficiency can be achieved on microscale devices.

Each of these parameters was shown to be significant in altering fluorination percentage for the on-chip optimization of [^{18}F]FDG, [^{18}F]FLT, [^{18}F]fallypride, and [^{18}F]SFB (Keng & van Dam, 2015). In contrast to the macroscale, reagent concentrations need to be modestly increased to offset the ~100–1000× scale down in reaction size (Koag et al., 2014a, 2014b). For example, the maximum fluorination efficiency of [^{18}F]FDG synthesis was reached, when reagent concentrations were increased by at least five times (Keng & van Dam, 2015).

Similarly, a reduction in droplet volume increased fluorination efficiency, provided that there was sufficient volume for the reaction mixture to be completely solvated for the entire length of the reaction (Keng & van Dam, 2015). For instance, reducing the droplet volume from 4 to 2 μL (while maintaining a twofold increase in the reagent concentrations), Javed et al. demonstrated an increase in fluorination efficiency during the synthesis of [^{18}F]FLT from 79 to 94% (Javed et al., 2014). The main reason behind this increase is shortening the duration of the fluorination and hydrolysis steps, thereby minimizing the potential loss of radioactivity due to droplet volatility or on-chip stiction events. Another example is Kim et al., where reducing droplet size from 6 to 2 μL removed the need to have a drying step after hydrolysis, since there was minimal residual DMSO remaining after fluorination. As a result, Kim et al. were able to reduce the combined heating time of a three-step radiosynthesis of [^{18}F]SFB by avoiding the long DMSO evaporation step, which led to an increase in the crude RCY from 38 to 50% (Kim et al., 2019).

Additionally, another factor that significantly alters fluorination efficiency is the phase transfer catalyst (PTC) to precursor ratio. As shown in Fig. 4a, during the synthesis of [^{18}F]SFB, Kim et al. had to deviate from standard macroscale PTC to precursor ratios of 4–6 and instead found optimal fluorination efficiency with a ratio of 2.3 (Kim et al., 2019). Furthermore, varying precursor amounts alone can affect the fluorination step—that is, the production of the [^{18}F]FTAG intermediate in [^{18}F]FDG synthesis was altered by varying only the amount of precursor available during the fluorination reaction (Keng et al., 2012), as illustrated in Fig. 4c.

At the microscale, the fluorination reaction time and reaction temperature stand as the main significant factors influencing fluorination efficiency. Both Kim et al. (2019) and Keng et al. (2012) showed the effects of reaction time (Fig. 4b and 4e) and temperature (Fig. 4d) on fluorination efficiency. From Kim et al. (2019), reaction times less than 4.5 min were generally shown to have demonstrably lower fluorination efficiencies, however, increasing reagent concentration can improve the fluorination efficiency. Accordingly, Keng et al. (2012) illustrated that increasing the reaction time can increase [^{18}F]FTAG conversion. As shown, adding more time (7 min) can further increase the efficiency from 56 % (1 min) to > 80 % (7 min) at a temperature of 100 °C (Fig. 4e). Although increasing reaction temperature from 80 to 100 °C can have the largest step increase in the [^{18}F]FTAG conversion efficiency from ~45 to 85% for a static reaction time of 7 min (Fig. 4d). This follows

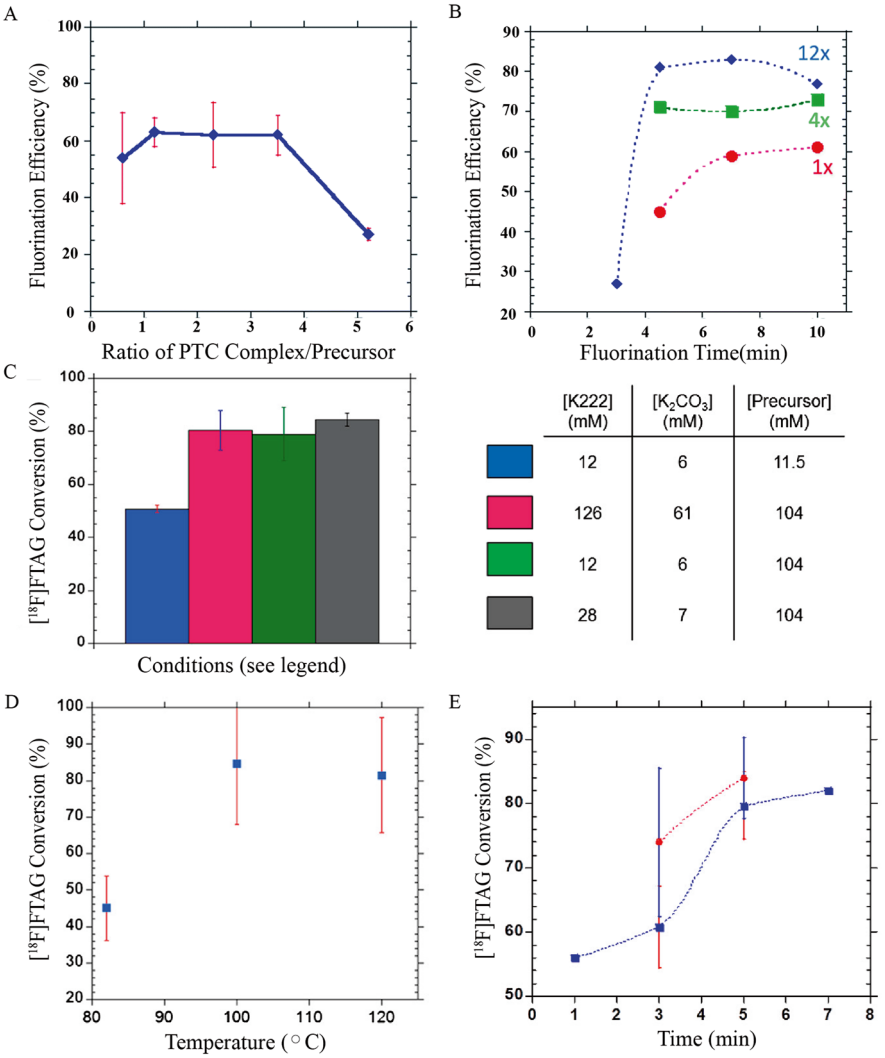

Fig. 4 Improving fluorination efficiency and radiochemical conversion. (**a**) Fluorination efficiency of [^{18}F]SFB as a function of PTC complex to precursor ratio (Kim et al., 2019). Permission obtained from the Royal Society of Chemistry. (**b**) Fluorination efficiency as a function of fluorination time for varied reagent concentrations (Kim et al., 2019). Permission obtained from the Royal Society of Chemistry. (**c**) Effects of reagent concentrations on fluorination efficiency during [^{18}F]FDG synthesis while temperature and reaction time remain constant at 90 °C and 5 min (Keng et al., 2012). Permission obtained from the Proceedings of the National Academy of Sciences. (**d**) Effect of temperature on [^{18}F]FTAG conversion efficiency for conserved reaction time of 5 min (Keng et al., 2012). Permission obtained from the Proceedings of the National Academy of Sciences. (**e**) Fluorination efficiency during [^{18}F]FDG intermediate synthesis for various reaction times (red circles indicate reactions performed at 100 °C, and blue squares indicate reactions performed at 120 °C) (Keng et al., 2012). (Permission obtained from the Proceedings of the National Academy of Sciences)

the goal for performing synthesis on the chip, which is to minimize the reaction time (and minimize decay) while maximizing the conversion efficiency.

3.2 Purification and DMF

Although the ideal scenario would be to purify the crude product on-chip, external analytical high-performance liquid chromatography (HPLC) has been widely used for the final purification of DMF reaction mixtures. This approach has several advantages over semi-preparative HPLC which is used in conjunction with macroscale syntheses, including the use of smaller diameter columns, which result in lower flow rates, improved separation compared to solid-phase extraction (SPE), narrower peak widths, and reduced eluent consumption (Chen et al., 2014a, 2014b; Bejot et al., 2011; Lebedev et al., 2013; Keng & van Dam, 2015; Wang et al., 2019, 2020; Kim et al., 2019; Shah et al., 2012). In some cases, such as with [^{18}F]fallypride and [^{18}F]SFB, where SPE was not feasible, analytical scale radio-HPLC was used for purification. This process involved separation using an analytical C-18 column with a specific mobile phase. Regarding [^{18}F]SFB, Kim et al. achieved a radiochemical purity exceeding 95% along with a radiochemical yield of 39 ± 7% (Kim et al., 2019), which is comparable to yields obtained through macroscale synthesis methods (Vaidyanathan & Zalutsky, 2006).

External purification via solid-phase extraction (SPE) or high-performance liquid chromatography (HPLC) adds size, cost, and complexity to the overall procedure (Keng & van Dam, 2015); however, miniaturizing these processes could alleviate these issues, and it can be truly an automated and compact system. As a result, Chen et al. designed a single microfluidic chip for labeling various radiotracers, upon which [^{18}F]FDG and [^{18}F]FLT were purified via an SPE cartridge (Chen et al. 2014b) that consisted of four different SPE sorbents. Javed et al. and Keng et al. also implemented similar SPE cartridges for the purification of [^{18}F]FLT and [^{18}F]FDG, respectively. A sample cartridge used for the purification [^{18}F]FLT is shown in Fig. 5a (Javed et al., 2014). Using such an off-chip purification approach for [^{18}F]FDG, Keng et al. were able to achieve a residual concentration of Krytofix less than 4 μg/mL as well as residual levels of DMSO, ethanol, and acetonitrile being 870 ppm, 115 ppm, and less than 20 ppm, respectively. All of these concentrations were well below the limit set by the United States Pharmacopeia. The overall radiochemical yield of [^{18}F]FDG was 22 ± 8% (Keng et al., 2012). Similarly, Javed et al. were able to obtain a RCY of 63 ± 5% for [^{18}F]FLT with over 99% radiochemical purity. The cartridge purification efficiency was 89 ± 2% (Javed et al., 2014). Nonetheless, the significant progress in miniaturization opens the possibility of integrating downstream processes on-chip, such as purification, which would play a crucial role in making decentralized PET production feasible in the laboratory setting.

Microscale purification solutions have been shown to completely automate the tracer synthesis workflow on chip with purification (Tarn et al., 2013; Chen et al.,

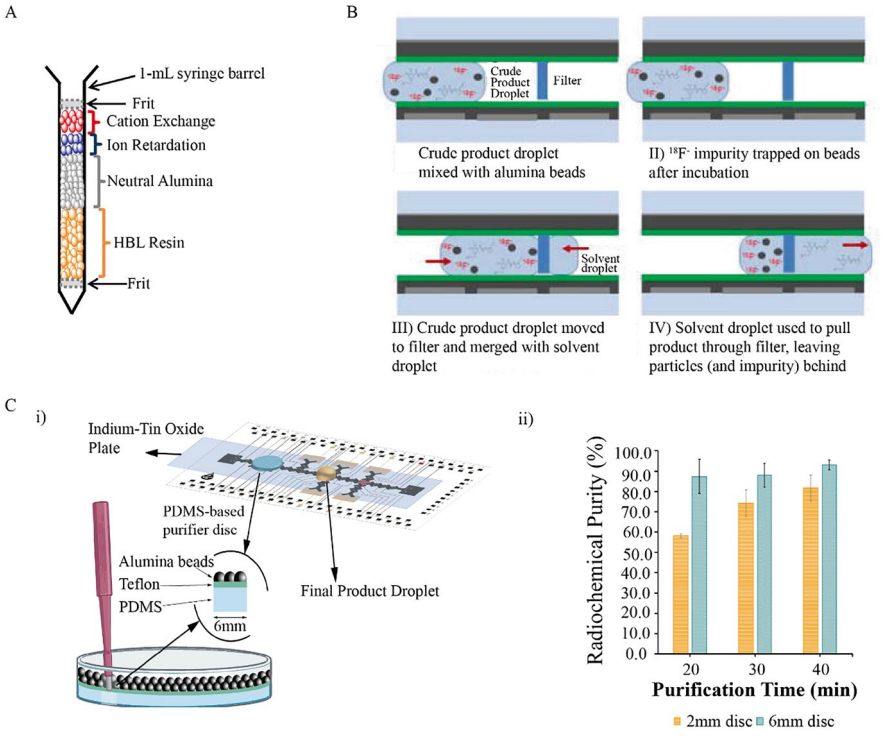

Fig. 5 Automating purification for on-chip synthesis. (**a**) Multilayered SPE purification cartridge for [^{18}F]FLT (Javed et al., 2014). Permission obtained from the Society of Nuclear Medicine and Molecular Imaging. (**b**) Workflow for on-chip SPE (Keng & van Dam, 2015). Permission obtained from Hindawi. (**c**) Using 2 and 6 mm PDMS disks for on-chip purification and their implications on RCY (Ahmadi et al., 2023). (Permission obtained from the Royal Society of Chemistry)

2014a, 2014b; Ahmadi et al., 2023). Primarily, Chen et al. demonstrated SPE on-chip via the integration (via photolithography) using KMPR® photoresist diamond shaped 140 μm tall pillars into top plate for the purification of [^{18}F]fallypride from [^{18}F]fluoride. These pillars served to mechanically separate the alumina particles, which were added after the reaction to scavenge unreacted [^{18}F]fluoride from the purified product (Chen et al., 2014a, 2014b). Although the particles and pillars served to eliminate [^{18}F]fluoride from the reaction mixture, they did not remove other impurities that may have been present. Figure 5b shows a methodological workflow for alumina bead separation using the fabricated pillars, and as shown, Chen et al. were able to achieve a removal of [^{18}F]fluoride to <1% (from the 16% in the crude product). In addition, the fluorination yield of 82% measured by Cerenkov imaging of activity in the purified product droplet versus activity trapped on the filtered alumina beads post-purification was consistent with the 83.9% measured radioactivity in the crude mixture via radio-TLC (Chen et al., 2014a, 2014b).

Similarly, Tarn et al. etched two glass plates and bonded them together to create a 300-μm-deep chamber non-DMF microfluidic device. The etched chambers were seeded with SPE particles and Teflon tubing was connected to drilled inlets and outlets to provide flow. Their chip was able to remove all [^{18}F]fluoride ions (from 25% in the crude product), increase [^{18}F]FDG radiochemical purity from 47% pre-purification to 86 ± 3% post-purification, and reduce partially hydrolyzed [^{18}F]FTAG from the hydrolysis reaction to 14 ± 3% (from 27% unpurified) (Tarn et al., 2013). We envision that such a channel-based platform could be combined with DMF, given the recent interest in integrating such platforms for high-throughput applications (Ahmadi et al., 2019; Samlali et al., 2020).

Finally, Ahmadi et al. developed 2 and 6 mm polydimethylsiloxane (PDMS)-based purifier disks coated with Teflon and alumina (as shown in Fig. 5c) to be placed on the DMF setup (Ahmadi et al., 2023). The crude product droplet was actuated onto these disks and incubated for up to 40 min to remove residual [^{18}F]fluoride and [^{18}F]FTAG (Ahmadi et al., 2023). While the incubation time is significantly longer than at the macroscale, the findings showed that a 6-mm purifier disk with a 40-min incubation time resulted in a radiochemical purity of ~93% (Ahmadi et al., 2023).

4 Future Trends in DMF and Radiochemistry

4.1 Machine Learning

Machine learning has emerged as a powerful tool for predicting the behavior of biochemical systems, enabling output predictions without the need for conducting an exhaustive library of experiments (Carbonell et al., 2019; Radivojević et al., 2020). Considering the necessity to finely adjust multiple parameters for radiotracer synthesis, the integration of machine learning offers a promising opportunity to improve radiolabeling efficiencies robustly. By inputting various previously measured conditions into a predictive model, the synthesis process can be optimized effectively.

In the past decade, considerable research efforts have focused on the use of machine learning and artificial intelligence to identify optimal sites for radiolabeling and reaction optimization (Bowden et al., 2019; Webb & Scott, 2021; Saboury et al., 2023). The advent of fully automated radiosynthesis systems has significantly expanded the capacity to conduct experiments and screen various conditions for optimization purposes. Recently, Ahmadi et al. presented a novel approach that combines radiochemistry, DMF, and machine learning to streamline the identification of a minimal number of experiments required for radiosynthesis optimization. The authors successfully demonstrated the integration of a one-factor at a time (OFAT) approach within the framework of radiochemistry, DMF, and machine learning. This innovative technique was employed to optimize the synthesis of

[^{18}F]FDG on a closed DMF platform, yielding promising results (Ahmadi et al., 2023). By obtaining a base level of reaction performance from literature for each factor, the value of one factor is changed, followed by measuring the output response (i.e., fluorination efficiency), and the process is repeated with another factor. After the values for each factor have been changed once, the output (fluorination efficiency in this case) of each case is compared to the base case via statistical analysis (t-test) to determine whether each of the parameters is significant or not. Figure 6a showcases eight experiments showing a value changed for each factor and the effect on the output fluorination efficiency for [^{18}F]FDG synthesis. The cumulative total of these trials, in addition to previously reported values, forms a training dataset. Finally, a multiple linear regression model was subsequently generated to predict optimal output values based on the training dataset generated (Ahmadi et al., 2023). The schematic of the model finding statistically significant parameters and optimizing synthesis conditions is shown in Fig. 6b.

Only five of the seven parameters showed a statistically significant impact on [^{18}F]FDG fluorination efficiency: precursor concentration, radiolabeling temperature, base concentration, deprotection time, and precursor-to-[^{18}F]fluoride volume ratio. Subsequently, the model determined the optimal values for each significant

A

	Mannose triflate volume / ^{19}F volume	Mannose triflate concentration (mM)	Radiolabeling temperature (°C)	Radiolabeling time (min)	NaOH concentration (M)	Deprotection temperature (°C)	Deprotection time (min)	Fluorination efficiency (%)
Base	1	30.00	85	5	1.00	25	5	61.27 ± 3.88 (n= 6)
	0.3	30.00	85	5	1.00	25	5	51.48 (0.0297)
	1	20.00	85	5	1.00	25	5	46.34 (0.0086)
	1	30.00	100	5	1.00	25	5	74.92 (0.0282)
	1	30.00	85	7	1.00	25	5	54.56 (0.0671)
	1	30.00	85	5	0.10	25	5	15.62 (0.0001)
	1	30.00	85	5	1.00	50	5	66.12 (0.2778)
	1	30.00	85	5	1.00	25	3	42.79 (0.0041)
Optimal	1	30.00	100	5	1.00	50	5	70.82 ± 1.54 (n=6)

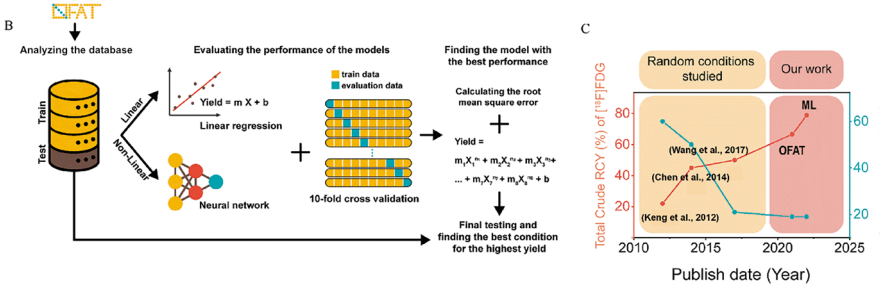

Fig. 6 Machine learning and DMF for radiochemistry. (**a**) Varying a single factor at a time (OFAT) and correlating each trial to fluorination efficiency (Ahmadi et al., 2023). Permission obtained from the Royal Society of Chemistry. (**b**) Schematic representation of using OFAT output to generate a predictive model to find significant parameters and optimal parameter values (Ahmadi et al., 2023). Permission obtained from the Royal Society of Chemistry. (**c**) Graphical illustration comparing the total crude radiochemical yield achieved by OFAT assay optimization (Ahmadi et al., 2023). (Permission obtained from the Royal Society of Chemistry)

parameter using a linear model equation predicted to obtain 85% fluorination efficiency, and the conditions were validated experimentally on-chip with a very similar (~84%) observed fluorination efficiency. Higher yields more than 85% were modeled, but the predicted experimental conditions (e.g., very high concentrations of NaOH) were not possible to be implemented on the chip (Ahmadi et al., 2023). However, using this optimization method, Fig. 6c demonstrates a decrease in synthesis time as well as an increase in synthesis yield compared to previous works. As this work was the first to integrate machine learning with radiotracer synthesis on DMF, the door opens to further leveraging machine learning either for optimization of [^{18}F]FDG using larger train-test datasets or the efficient synthesis of other tracers.

4.2 Moving DMF from Bench to Practice

Moving toward a decentralized platform for synthesis is to construct a DMF platform to be fully automated and miniaturized for easy adoption across various hospitals. Narahari et al. were able to create a fully encapsulated DMF system including all essential and peripheral electronics for patient sample processing in screening for Zika (Narahari et al., 2022). Their entire DMF platform was a box 26 cm in length by 22 cm in width allowing for portability and versatility (Narahari et al., 2022). The implementation of such an encompassing system for DMF radiotracer synthesis could aid in truly burgeoning adoption across testing facilities.

Similarly, although solutions have been demonstrated in creating a world-to-chip interface (Shah et al., 2013; Moazami et al., 2019; Perry et al., 2021), further development and integration of world-to-chip systems in encapsulated platforms like that of Narahari et al. are needed for an accurate and automated system to prevent manual handling of radioactive chemicals. In addition, the use of harsh chemicals deteriorating chip surfaces represents a barrier toward adoption of decentralized synthesis (Ahmadi et al., 2023). The use of removable dielectrics, particularly when dealing with harsh chemicals like those used for tracer synthesis, can allow for the reusability of the bottom plate and thus reduce reusability concerns and dielectric breakdown concerns (Freire 2016; Yang et al., 2009; Xing et al., 2021).

Furthermore, every DMF system discussed except for Mogi et al. uses a glass substrate, and electrodes are patterned prior to dielectric coating. These processes require an expensive, well-equipped clean room along with costly materials (Jain et al., 2017). Alternative methods of generating lower cost DMF systems with merge, mix, dispense, and split could leverage printed circuit boards (PCBs) with Parylene-C or PDMS as a dielectric (Abdelgawad & Wheeler, 2008; Gong & Kim, 2008; Jain et al., 2017; Perry et al., 2021) or thin-film transistor-based technologies (Anderson et al., 2021; Luo et al., 2022). As such, more cost-effective solutions would need to be leveraged to make DMF chips less expensive and more viable for mass production and readily available for automated radiotracer synthesis.

References

Abadian, A., Sepehri Manesh, S., & Jafarabadi Ashtiani, S. (2017). Hybrid paper-based microfluidics: Combination of paper-based analytical device (μPAD) and digital microfluidics (DMF) on a single substrate. *Microfluidics and Nanofluidics, 21*, 1–11.

Abdelgawad, M., & Wheeler, A. R. (2008). Low-cost, rapid-prototyping of digital microfluidics devices. *Microfluidics and Nanofluidics, 4*, 349–355.

Ahmadi, F., Samlali, K., Vo, P. Q., & Shih, S. C. (2019). An integrated droplet-digital microfluidic system for on-demand droplet creation, mixing, incubation, and sorting. *Lab on a Chip, 19*(3), 524–535.

Ahmadi, F., Simchi, M., Perry, J. M., Frenette, S., Benali, H., Soucy, J. P., Massarweh, G., & Shih, S. C. (2023). Integrating machine learning and digital microfluidics for screening experimental conditions. *Lab on a Chip, 23*(1), 81–91.

Anderson, S., Hadwen, B., & Brown, C. (2021). Thin-film-transistor digital microfluidics for high value in vitro diagnostics at the point of need. *Lab on a Chip, 21*(5), 962–975.

Ashraf, M. A., & Goyal, A. (2023). Fludeoxyglucose (18F). In *StatPearls*. StatPearls Publishing. Retrieved from https://www.ncbi.nlm.nih.gov/books/NBK557653/.

Audrain, H. (2007). Positron emission tomography (PET) and microfluidic devices: A breakthrough on the microscale? *Angewandte Chemie International Edition, 46*(11), 1772–1775.

Bejot, R., Elizarov, A. M., Ball, E., Zhang, J., Miraghaie, R., Kolb, H. C., & Gouverneur, V. (2011). Batch-mode microfluidic radiosynthesis of N-succinimidyl-4-[18F]fluorobenzoate for protein labelling. *Journal of Labelled Compounds and Radiopharmaceuticals, 54*(3), 117–122.

Bowden, G. D., Pichler, B. J., & Maurer, A. (2019). A design of experiments (DoE) approach accelerates the optimization of copper-mediated 18F-fluorination reactions of arylstannanes. *Scientific Reports, 9*(1), 1–10.

Calderwood, S., Collier, T. L., Gouverneur, V., Liang, S. H., & Vasdev, N. (2015). Synthesis of 18F-arenes from spirocyclic iodonium (III) ylides via continuous-flow microfluidics. *Journal of Fluorine Chemistry, 178*, 249–253.

Carbonell, P., Radivojevic, T., & Garcia Martin, H. (2019). Opportunities at the intersection of synthetic biology, machine learning, and automation. *ACS Synthetic Biology, 8*(7), 1474–1477.

Chen, S., Javed, R., Lei, J., Kim, H. K., Flores, G., van Dam, R. M., Keng, P. Y., & Kim, C. J. (2012a, June). Synthesis of diverse tracers on EWOD microdevice for positron emission tomography (PET). In *Technical digest of the solid-state sensor and actuator workshop, Hilton Head Island, SC, USA*, pp. 3–7.

Chen, S., Lei, J., van Dam, R. M., Keng, P. Y., & Kim, C. J. (2012b, October). Planar alumina purification of 18F-labeled radiotracer synthesis on EWOD chip for positron emission tomography (PET). In *16th international conference on miniaturized systems for chemistry and life sciences (mTAS)*, pp. 1771–1773.

Chen, S., Dooraghi, A. A., Lazari, M., van Dam, R. M., Chatziioannou, A. F., & Kim, C. J. C. (2014a). On-chip product purification for complete microfluidic radiotracer synthesis. In *2014 IEEE 27th international conference on micro electro mechanical systems (MEMS)* (pp. 284–287). IEEE.

Chen, S., Javed, M. R., Kim, H. K., Lei, J., Lazari, M., Shah, G. J., van Dam, R. M., & Keng, P. Y. (2014b). Radiolabelling diverse positron emission tomography (PET) tracers using a single digital microfluidic reactor chip. *Lab on a Chip, 14*(5), 902–910.

Choi, K., Ng, A. H., Fobel, R., & Wheeler, A. R. (2012). Digital microfluidics. *Annual Review of Analytical Chemistry, 5*, 413–440.

Ding, H., Sadeghi, S., Shah, G. J., Chen, S., Keng, P. Y., & van Dam, R. M. (2012). Accurate dispensing of volatile reagents on demand for chemical reactions in EWOD chips. *Lab on a Chip, 12*(18), 3331–3340.

Elizarov, A. M., van Dam, R. M., Shin, Y. S., Kolb, H. C., Padgett, H. C., Stout, D., Shu, J., Huang, J., Daridon, A., & Heath, J. R. (2010). Design and optimization of coin-shaped microreactor chips for PET radiopharmaceutical synthesis. *Journal of Nuclear Medicine, 51*(2), 282–287.

Fobel, R., Fobel, C., & Wheeler, A. R. (2013). DropBot: An open-source digital microfluidic control system with precise control of electrostatic driving force and instantaneous drop velocity measurement. *Applied Physics Letters, 102*(19).

Freire, S. L. (2016). Perspectives on digital microfluidics. *Sensors and Actuators A: Physical, 250*, 15–28.

Gillies, J. M., Prenant, C., Chimon, G. N., Smethurst, G. J., Dekker, B. A., & Zweit, J. (2006). Microfluidic technology for PET radiochemistry. *Applied Radiation and Isotopes, 64*(3), 333–336.

Gong, J., & Kim, C. J. (2008). Direct-referencing two-dimensional-array digital microfluidics using multilayer printed circuit board. *Journal of Microelectromechanical Systems, 17*(2), 257–264.

Huang, T. W., Lin, C. H., & Ho, T. Y. (2010). A contamination aware droplet routing algorithm for the synthesis of digital microfluidic biochips. *IEEE Transactions on Computer-Aided Design of Integrated Circuits and Systems, 29*(11), 1682–1695.

Jain, V., Raj, T. P., Deshmukh, R., & Patrikar, R. (2017). Design, fabrication and characterization of low cost printed circuit board based EWOD device for digital microfluidics applications. *Microsystem Technologies, 23*, 389–397.

Javed, M. R., Chen, S., Kim, H. K., Wei, L., Czernin, J., van Dam, R. M., & Keng, P. Y. (2014). Efficient radiosynthesis of 3′-deoxy-3′-18F-fluorothymidine using electrowetting-on-dielectric digital microfluidic chip. *Journal of Nuclear Medicine, 55*(2), 321–328.

Jebrail, M. J., Ng, A. H., Rai, V., Hili, R., Yudin, A. K., & Wheeler, A. R. (2010). Synchronized synthesis of peptide-based macrocycles by digital microfluidics. *Angewandte Chemie, 122*(46), 8807–8811.

Jebrail, M. J., Renzi, R. F., Sinha, A., Van De Vreugde, J., Gondhalekar, C., Ambriz, C., Meagher, R. J., & Branda, S. S. (2015). A solvent replenishment solution for managing evaporation of biochemical reactions in air-matrix digital microfluidics devices. *Lab on a Chip, 15*(1), 151–158.

Keng, P. Y., & van Dam, R. M. (2015). Digital microfluidics: A new paradigm for radiochemistry. *Molecular Imaging, 14*(12), 7290–2015.

Keng, P. Y., Chen, S., Ding, H., Sadeghi, S., Shah, G. J., Dooraghi, A., Phelps, M. E., Satyamurthy, N., Chatziioannou, A. F., Kim, C. J. C., & van Dam, R. M. (2012). Micro-chemical synthesis of molecular probes on an electronic microfluidic device. *Proceedings of the National Academy of Sciences, 109*(3), 690–695.

Kim, H. K., Javed, M. R., Chen, S., Zettlitz, K. A., Collins, J., Wu, A. M., van Dam, R. M., & Keng, P. Y. (2019). On-demand radiosynthesis of N-succinimidyl-4-[18F]fluorobenzoate ([18F]SFB) on an electrowetting-on-dielectric microfluidic chip for 18 F-labeling of protein. *RSC Advances, 9*(55), 32175–32183.

Kimura, H., Tomatsu, K., Saiki, H., Arimitsu, K., Ono, M., Kawashima, H., Iwata, R., Nakanishi, H., Ozeki, E., Kuge, Y., & Saji, H. (2016). Continuous-flow synthesis of N-succinimidyl 4-[18F]fluorobenzoate using a single microfluidic chip. *PLoS One, 11*(7), e0159303.

Koag, M. C., Kim, H. K., & Kim, A. S. (2014a). Efficient microscale synthesis of [18F]-2-fluoro-2-deoxy-d-glucose. *Chemical Engineering Journal, 258*, 62–68.

Koag, M. C., Kim, H. K., & Kim, A. S. (2014b). Fast and efficient microscale radiosynthesis of 3′-deoxy-3′-[18F]fluorothymidine. *Journal of Fluorine Chemistry, 166*, 104–109.

Lebedev, A., Miraghaie, R., Kotta, K., Ball, C. E., Zhang, J., Buchsbaum, M. S., Kolb, H. C., & Elizarov, A. (2013). Batch-reactor microfluidic device: First human use of a microfluidically produced PET radiotracer. *Lab on a Chip, 13*(1), 136–145.

Lee, C. C., Sui, G., Elizarov, A., Shu, C. J., Shin, Y. S., Dooley, A. N., Huang, J., Daridon, A., Wyatt, P., Stout, D., & Kolb, H. C. (2005). Multistep synthesis of a radiolabeled imaging probe using integrated microfluidics. *Science, 310*(5755), 1793–1796.

Li, J. (2020). Current commercialization status of electrowetting-on-dielectric (EWOD) digital microfluidics. *Lab on a Chip, 20*(10), 1705–1712.

Liang, S. H., Yokell, D. L., Jackson, R. N., Rice, P. A., Callahan, R., Johnson, K. A., Alagille, D., Tamagnan, G., Collier, T. L., & Vasdev, N. (2014a). Microfluidic continuous-flow radiosynthesis of [18F]FPEB suitable for human PET imaging. *Medicinal Chemistry Communication, 5*(4), 432–435.

Liang, S. H., Yokell, D. L., Normandin, M. D., Rice, P. A., Jackson, R. N., Shoup, T. M., Brady, T. J., Fakhri, G. E., Collier, T. L., & Vasdev, N. (2014b). First human use of a radiopharmaceutical prepared by continuous-flow microfluidic radiofluorination: Proof of concept with the tau imaging agent [18F]T807. *Molecular Imaging, 13*(8), 7290–2014.

Liu, X., Ma, D., Ye, H., Hou, Y., Bai, X., Xing, Y., Cheng, X., Lin, B., & Lu, Y. (2023). Electrowetting-based digital microfluidics: Toward a full-functional miniaturized platform for biochemical and biological applications. *TrAC Trends in Analytical Chemistry*, 117153.

Luo, Z., Xu, J., Pan, Z., Yin, H., Cao, L., Zhou, G., & Liu, S. (2022). Programmable high integration and resolution digital microfluidic device driven by thin film transistor arrays. *IEEE Access, 10*, 30573–30582.

Moazami, E., Perry, J. M., Soffer, G., Husser, M. C., & Shih, S. C. (2019). Integration of world-to-chip interfaces with digital microfluidics for bacterial transformation and enzymatic assays. *Analytical Chemistry, 91*(8), 5159–5168.

Mogi, K., Kimura, H., Kondo, Y., Inoue, T., Adachi, S., & Natsume, T. (2021). Automatic radioisotope manipulation for small amount of nuclear medicine using an EWOD device with a dimple structure. *Royal Society Open Science, 8*(5), 201809.

Moon, H., Wheeler, A. R., Garrell, R. L., & Loo, J. A. (2006). An integrated digital microfluidic chip for multiplexed proteomic sample preparation and analysis by MALDI-MS. *Lab on a Chip, 6*(9), 1213–1219.

Narahari, T., Dahmer, J., Sklavounos, A., Kim, T., Satkauskas, M., Clotea, I., Ho, M., Lamanna, J., Dixon, C., Rackus, D. G., & da Silva, S. J. R. (2022). Portable sample processing for molecular assays: Application to Zika virus diagnostics. *Lab on a Chip, 22*(9), 1748–1763.

Perry, J. M., Soffer, G., Jain, R., & Shih, S. C. (2021). Expanding the limits towards 'one-pot' DNA assembly and transformation on a rapid-prototype microfluidic device. *Lab on a Chip, 21*(19), 3730–3741.

Radivojević, T., Costello, Z., Workman, K., & Garcia Martin, H. (2020). A machine learning automated recommendation tool for synthetic biology. *Nature Communications, 11*(1), 4879.

Ruecha, N., Lee, J., Chae, H., Cheong, H., Soum, V., Preechakasedkit, P., Chailapakul, O., Tanev, G., Madsen, J., Rodthongkum, N., & Kwon, O. S. (2017). Paper-based digital microfluidic chip for multiple electrochemical assay operated by a wireless portable control system. *Advanced Materials Technologies, 2*(3), 1600267.

Saboury, B., Bradshaw, T., Boellaard, R., Buvat, I., Dutta, J., Hatt, M., Jha, A. K., Li, Q., Liu, C., McMeekin, H., & Morris, M. A. (2023). Artificial intelligence in nuclear medicine: Opportunities, challenges, and responsibilities toward a trustworthy ecosystem. *Journal of Nuclear Medicine, 64*(2), 188–196.

Samlali, K., Ahmadi, F., Quach, A. B., Soffer, G., & Shih, S. C. (2020). One cell, one drop, one click: Hybrid microfluidics for mammalian single cell isolation. *Small, 16*(34), 2002400.

Selivanova, S. V., Mu, L., Ungersboeck, J., Stellfeld, T., Ametamey, S. M., Schibli, R., & Wadsak, W. (2012). Single-step radiofluorination of peptides using continuous flow microreactor. *Organic & Biomolecular Chemistry, 10*(19), 3871–3874.

Shah, G. J., Lei, J., Chen, S., Kim, C. J., Keng, P. Y., & van Dam, R. M. (2012). Automated injection from EWOD digital microfluidic chip into HPLC purification system. In *Proceedings of international conference on miniaturized systems for chemistry and life sciences (mTAS)*, pp. 356–358.

Shah, G. J., Ding, H., Sadeghi, S., Chen, S., & van Dam, R. M. (2013). On-demand droplet loading for automated organic chemistry on digital microfluidics. *Lab on a Chip, 13*(14), 2785–2795.

Tarn, M. D., Pascali, G., De Leonardis, F., Watts, P., Salvadori, P. A., & Pamme, N. (2013). Purification of 2-[18F]fluoro-2-deoxy-d-glucose by on-chip solid-phase extraction. *Journal of Chromatography A, 1280*, 117–121.

Vaidyanathan, G., & Zalutsky, M. R. (2006). Synthesis of N-succinimidyl 4-[18F]fluorobenzoate, an agent for labeling proteins and peptides with 18F. *Nature Protocols, 1*(4), 1655–1661.

Vaquero, J. J., & Kinahan, P. (2015). Positron emission tomography: Current challenges and opportunities for technological advances in clinical and preclinical imaging systems. *Annual Review of Biomedical Engineering, 17*, 385–414.

Walters, L. R., Martin, K. J., Jacobson, M. S., Hung, J. C., & Mosman, E. A. (2012). goya. *Journal of Nuclear Medicine Technology, 40*(1), 52–56.

Wang, J., Chao, P. H., & van Dam, R. M. (2019). Ultra-compact, automated microdroplet radiosynthesizer. *Lab on a Chip, 19*(14), 2415–2424.

Wang, J., Chao, P. H., Slavik, R., & van Dam, R. M. (2020). Multi-GBq production of the radiotracer [18F]fallypride in a droplet microreactor. *RSC Advances, 10*(13), 7828–7838.

Webb, E. W., & Scott, P. J. (2021). Potential applications of artificial intelligence and machine learning in radiochemistry and radiochemical engineering. *PET Clinics, 16*(4), 525–532.

Xing, Y., Liu, Y., Chen, R., Li, Y., Zhang, C., Jiang, Y., Lu, Y., Lin, B., Chen, P., Tian, R., & Liu, X. (2021). A robust and scalable active-matrix driven digital microfluidic platform based on printed-circuit board technology. *Lab on a Chip, 21*(10), 1886–1896.

Yang, H., Luk, V. N., Abelgawad, M., Barbulovic-Nad, I., & Wheeler, A. R. (2009). A world-to-chip interface for digital microfluidics. *Analytical Chemistry, 81*(3), 1061–1067.

Zhang, X., Liu, F., Knapp, K. A., Nickels, M. L., Manning, H. C., & Bellan, L. M. (2018). A simple microfluidic platform for rapid and efficient production of the radiotracer [18F]fallypride. *Lab on a Chip, 18*(9), 1369–1377.